JOURNAL OF MATERIALS SCIENCE 18 (1983) 2798–2810

Propagation of stress corrosion cracks in aligned glass fibre composite materials

J. N. PRICE, D. HULL
Department of Metallurgy and Materials Science, University of Liverpool, PO Box 147, Liverpool, UK

A modified fracture toughness test has been used to measure the growth of cracks in unidirectional glass fibre/polyester resin composite materials in the presence of a dilute hydrochloric acid. Crack growth rates perpendicular to the fibre axis have been measured over a range of stress intensities. Scanning electron microscope studies of the fracture surfaces have shown that the micromechanisms of nucleation and propagation are dependent on stress intensity. The use of crack growth data to predict component lifetimes and the existence of inherent flaws in the material are discussed.

1. Introduction

Under the combined influence of a stress and a corrosive environment glass fibre-reinforced plastics (GRP) may fail at much lower stresses than in the absence of the environment. This phenomenon has been called stress or strain corrosion. Metcalfe and his colleagues [1, 2] have shown that spontaneous cracking of glass fibres occurs in acids even in the absence of an externally applied stress. They attributed this to an ion exchange process in which the metal ions in the glass are replaced by hydrogen ions from the acid. The subsequent shrinkage of the outer layer of the fibre results in surface tensile stresses which lead to failure. Alternative explanations of spontaneous cracking based on leaching of the material at the tip of pre-existing flaws and changes in the surface tension of crack surfaces have been proposed, see for example [3] and [4]. In the presence of an applied stress the strength of single glass fibres and fibre bundles is time dependent. The effect is most pronounced when the fibres are immersed in mineral acids [5] but significant reductions have been observed in distilled water [6]. Aveston *et al.* [7] have proposed a detailed model for failure of fibre bundles in a corrosive environment based on the kinetics of crack growth in individual fibres and the statistics of bundle failure.

In composite materials the fibres are protected from the environment by the resin matrix. The degree of protection depends on the permeability of the resin to the diffusion of active species from the environment and the ability of the resin to resist premature cracking which would allow the environment to come into direct contact with the fibres. Hogg and Hull [8] have shown that stress corrosion of GRP can occur in the absence of prior resin cracking. Extensive studies have been made of the mode of crack growth and the effect of fibre arrangement and resin properties [9, 10]. A model for stress corrosion based on the effects of resin diffusion and the combined effects of resin fracture and fibre fracture has been proposed [8]. A feature of the model is that stress corrosion cracking is strongly dependent on the stress parallel to the fibres. This is particularly true under conditions where premature resin cracking does not occur.

Stress corrosion cracking is characterized by the formation of a planar crack which usually grows at right angles to the principal fibre direction. The rate of growth depends on the applied stress and the environment. Consequently, the lifetime of a component or structure made from GRP, subjected to stress corrosion conditions, can be predicted provided the dependence of crack growth rate on stress intensity at the crack tip is known.

In a critical review of the application of fracture mechanics to the growth of cracks in com-

0022–2461/83 $03.00 + .12

posite materials, Kanninen *et al.* [11] have highlighted the difficulties of applying linear elastic fracture mechanics (LEFM) to these materials. Apart from the high degree of anisotropy in most composite materials, which complicates the stress analysis, there is the major problem that the damage zone at the crack tip often extends over a large volume of the material thus invalidating the approach. The damage zone in stress corrosion fracture of GRP is small, particularly in the early stages of fracture, so that the use of LEFM appears to be valid. A similar approach has been adopted recently by Aveston and Sillwood [12] and their results are discussed later.

2. Fracture mechanics analysis

The simple equations relating the stress intensity for mode I opening, K_I, to the specimen geometry for homogeneous, isotropic materials cannot be applied directly to composite materials because they are usually non-homogeneous and anisotropic. Indeed, the determination of a meaningful value of K_I is likely to prove very difficult and in some cases intractable. For the purpose of this work the strain energy release rate G is used as a primary parameter and values of K_I are derived from the plane strain equation

$$K_I^2 = EG/(1-\nu^2) \tag{1}$$

assuming that the relevant values of Young's modulus E and Poisson's ratio ν for the test specimen geometry used are the Young's modulus parallel to the fibres $E_{\parallel}$ and $\nu_{\parallel\perp}$ respectively. The difficulty remains of selecting the most appropriate values of E and ν to use when other test specimen geometries and materials are used.

To pursue this approach the test sample is calibrated by determining experimentally the change in compliance C with crack length a and obtaining G from

$$G = \frac{P^2}{2t}\left(\frac{dC}{da}\right) \tag{2}$$

where P is the applied load and t the width of the crack. Hence from Equation 1

$$K_I^2 = \left(\frac{E}{1-\nu^2}\right)\left(\frac{P^2}{2t}\right)\frac{dC}{da} \tag{3}$$

or, alternatively

$$K_I = Y\frac{Pa^{1/2}}{tW} \tag{4}$$

where W is the specimen length and the geometrical factor Y is given by

$$Y = \left[\frac{Et}{2(1-\nu^2)(a/W)}\frac{dC}{d(a/W)}\right]^{1/2} \tag{5}$$

For grooved specimens in which the total width of the specimen, t, is greater than the width of the crack front in the groove, t_g, it is usual practice to replace t in Equation 5 by $(t\,t_g)^{1/2}$.

The shape of the fracture mechanics test specimen used in this work is illustrated in Fig. 1. For reasons which are explained later, the specimen has a laminated construction with a centre groove along the direction of crack growth at right angles to the loading direction. To measure the crack growth rate da/dt under conditions where the driving force is constant, it is necessary to shape the specimen so that G and hence K_I is independent of crack length for a constant applied load. This has been achieved with limited success using trial and error methods by measuring G at differ-

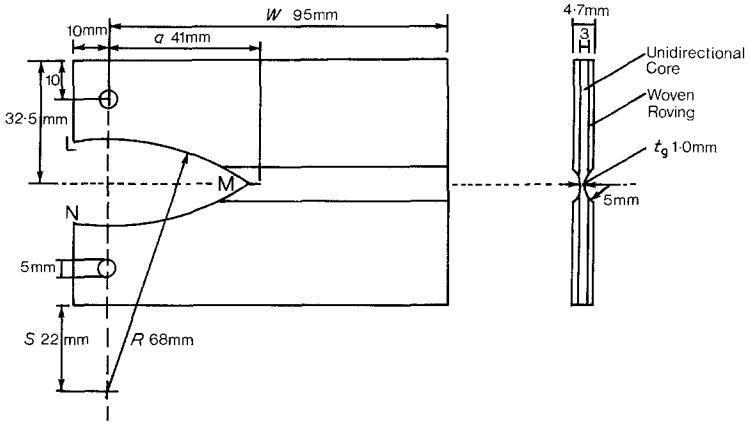

Figure 1 Shape and dimensions of test specimens.

ent artificial crack lengths, a, for a series of specimens with different values of S and R (see Fig. 1).

The values of G and K_I were determined from the specimen compliance (see Equations 2 and 3) which was measured using an Instron 1185 testing machine. For calibration purposes the artificial crack was introduced using a fine saw blade. The change of K_I with total effective crack length a is shown in the K_I calibration curves in Fig. 2 for three different specimens. K_I/P varies with a/W for all three specimens but for specimen B it is approximately constant in the range $0.40 < a/W < 0.53$. This specimen geometry was selected for the stress corrosion tests.

The crack opening displacement (COD) was measured during compliance testing, using a clip-on COD gauge, to obtain the relationship between COD and crack length. This relationship provides an independent, though indirect method, of measuring the crack length during stress corrosion cracking. Since COD can be measured continuously during crack growth, the approach is a useful complement to the non-continuous direct observation methods.

3. Experimental methods and materials

All the tests were made on unidirectionally aligned glass fibres in a polyester resin matrix. Fibreglass Equirove 2400 tex glass fibre rovings and Scott Bader Crystic 272 resin with 0.5% cobalt naphthanate accelerator and 1% methyl ethyl ketone peroxide catalyst, were used to fabricate the composite materials.

The unidirectional laminae were made by passing the glass roving through a resin bath and winding it onto a flat plate mandrel using a filament winding machine [13]. After winding, the mandrel was compressed between steel plates and the material cured to produce a void-free composite with a uniform volume fraction V_f. The volume fraction was controlled by the amount of resin squeezed out during the compression stage. In these experiments $V_f = 0.48$ and 0.57 were used. Unidirectional material was laminated with woven glass roving and Crystic 272 resin to produce a balanced laminate which was given a final post-cure for 12 h at 50° C.

The test pieces (see Fig. 1) were cut from the laminate using a steel template and a fine tooth

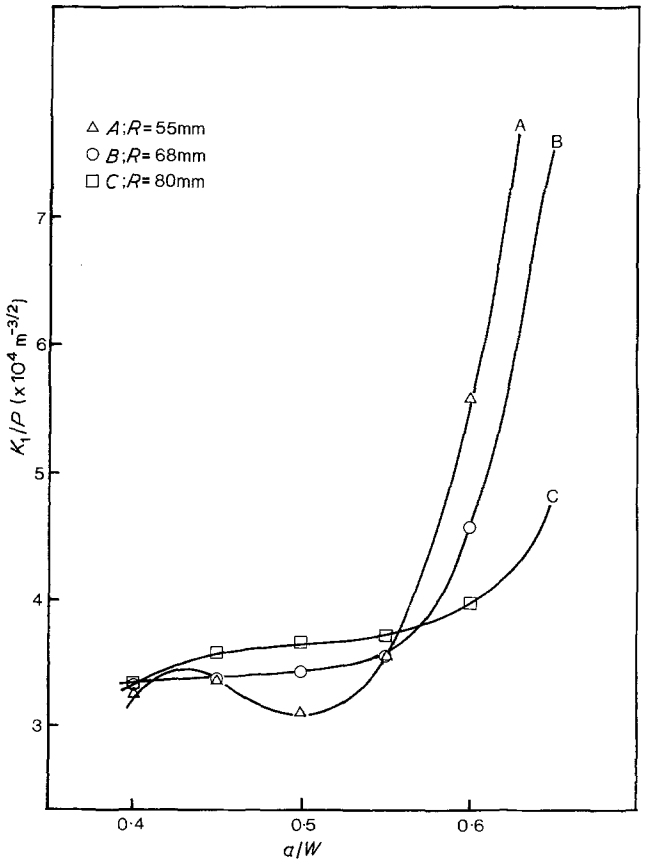

Figure 2 Variation of K_I with crack length for different values of specimen-shape parameters S and R.

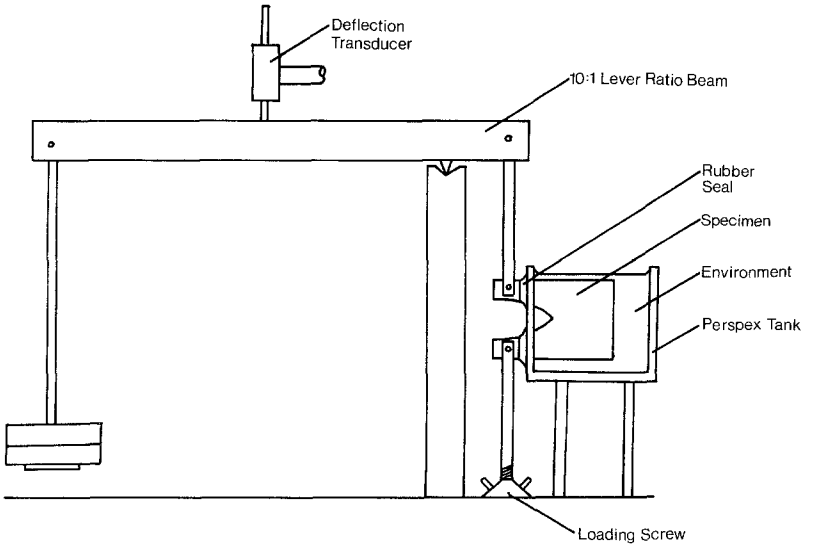

Figure 3 Schematic illustration of test rig used for crack growth experiments.

saw. The specimens were grooved along their centre line using a milling machine. The woven roving and the groove prevented extensive failure, owing to transverse cracking parallel to the fibre direction, by stiffening the beam and reducing the crack width. After the notch LM–MN (Fig. 1) had been cut, the crack tip was formed using a fine saw followed by notching with a sharp scalpel blade. This procedure helped to minimize the time required to produce a sharp stress corrosion crack. All the cut surfaces were ground to ensure accurate specimen dimensions. In the initial experiments it was found, from an examination of the fracture surfaces, that acid attack occurred at the sides of the specimen as well as at the tip of the notch. This was prevented in later tests by coating the sides of the specimen with grease.

The tests were carried out at constant load using modified creep rigs with a 10:1 lever ratio as illustrated in Fig. 3. The specimen and the corrosive environment are contained within a perspex tank. The loading arms pass through the tank walls and are sealed by latex rubber sleeves. Crack growth was observed directly using transmitted light and a travelling microscope. The crack front was well defined and its position was measured to within 0.1 mm. The crack opening displacement was monitored continuously using a linear voltage displacement transducer acting at the loading arm. The transducer output was recorded using a microprocessor system.

Previous work has shown that the stress corrosion effect depends on the concentration and type of acid used [14]. This work has been restricted to 0.6 M HCl and all the tests were carried out at 20 ± 2° C.

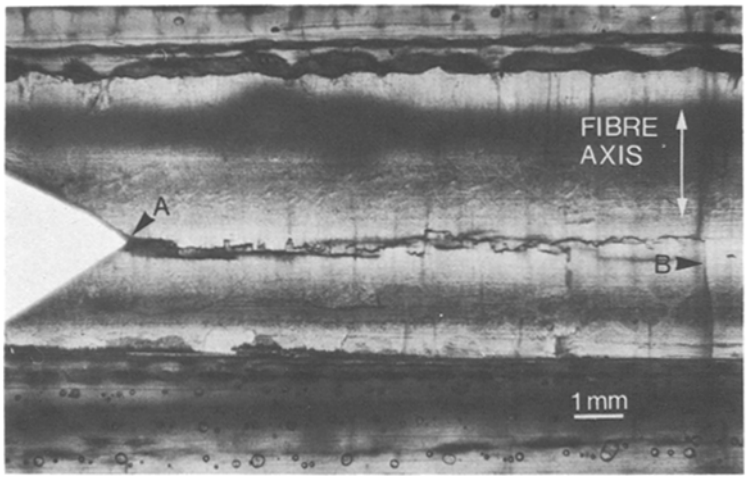

Figure 4 Side view of stress corrosion crack.

4. Results

The general appearance of a stress corrosion crack which has grown from the root of a notch is shown in Fig. 4. The crack has propagated from the notch at A normal to the fibre direction. Apart from some small steps, crack growth is planar. Planar growth terminated at B owing to the formation of a transverse crack parallel to the fibres.

A typical curve showing the change in crack length with time is shown in Fig. 5a. The crack length, which was obtained from COD measurements, increases in an irregular way but the general slope of the curve is approximately constant. This indicates that on a macroscopic scale the crack growth rate is constant but on a microscopic scale there are large variations. These variations relate to the mechanism of crack extension and are associated particularly with secondary cracking parallel to the fibres, as illustrated in Fig. 5b. There is close correlation between the steps on the fracture surface at, for example, B and B′ and the shape of the crack growth curve. The occurrence of secondary cracking leads to a decrease in the crack growth rate.

A series of crack growth curves for specimens with different applied loads is shown in Fig. 6. The continuous curves were obtained from COD measurements and the compliance calibration and the individual points are from direct measurements of crack length obtained using a travelling microscope. The agreement between the two methods is good indicating that the continuous measurement COD approach can be used to obtain fine detail of crack growth rate characteristics. Implicit in the use of COD measurements to determine crack length is the assumption that the crack tip geometry remains constant throughout the test. Transverse cracking at the crack tip will

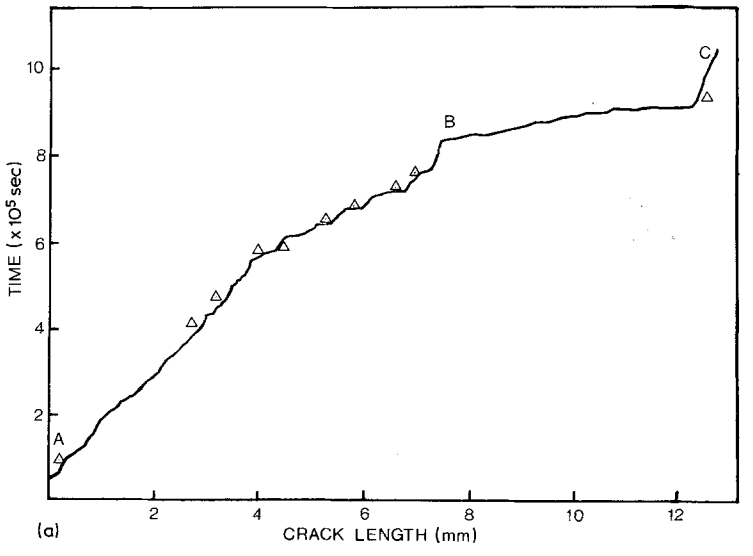

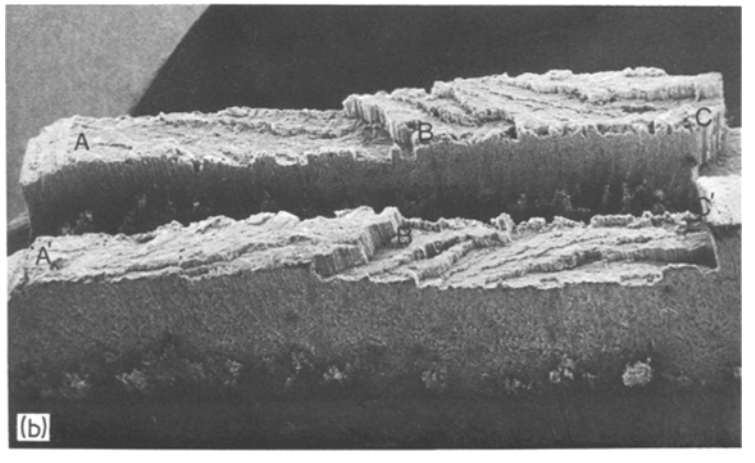

Figure 5 (a) Typical curve showing variation of crack length with time, ($G = 0.9\,\mathrm{kJ\,m^{-2}}$). (b) Scanning electron micrographs of opposite fracture surfaces of specimen used for test in (a).

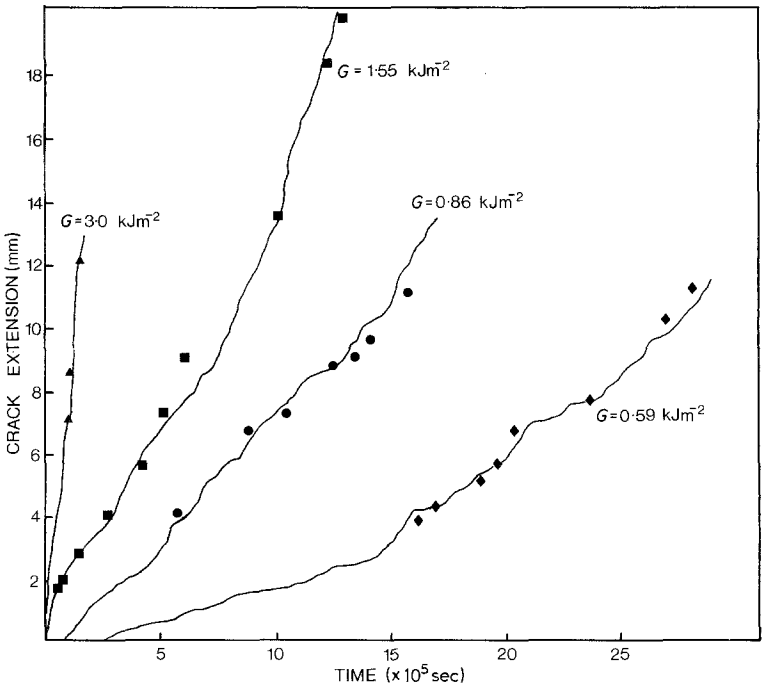

Figure 6 Variation of crack length with time for different values of K_I. A continuous line was obtained from COD measurements and individual points from direct observations.

undoubtedly change the shape of the crack, but the close agreement shown in Fig. 6 indicates that the amout of transverse cracking in these experiments is insufficient to invalidate the COD approach although it must lead to some modification of the crack growth kinetics.

Although the curves in Fig. 6 have approximately constant slope, there is some increase in slope at longer crack lengths. This is almost certainly due to the small changes in stress intensity with crack length evident in the calibration curves shown in Fig. 2. The curves show a delay time before crack growth begins for tests with low values of G, which is presumably due to the time taken in establishing a sharp stress corrosion crack at the tip of the razor cut. The delay time increases with decreasing G. The variation in crack growth rate with G and K_I is shown in Fig. 7. The rate was obtained from curves, such as those in Fig. 6 in the region where G was approximately constant. The variations in macroscopic growth rates within a single test are shown by the bar lines. The effect of volume fraction of fibres is also illustrated in Fig. 7; an increase in V_f results in a decrease in crack growth rate for a given value of G.

The general appearance of the fracture surface of a crack which has grown at constant G (Fig. 5b) is independent of position except in the nucleation region (A in Fig. 5b). In this region the fracture surface is extremely smooth (Fig. 8) with only isolated fibres showing out-of-plane fracture. The amount of out-of-plane fracture increases away from the nucleation region and there is a marked change in the appearance of the fracture surfaces of fibres and resin.

The fracture surface of each fibre is characterized by a very smooth mirror region surrounded by a hackle region. The direction of crack growth is readily deduced from the position of the river lines in the hackle regions as illustrated in Fig. 9. By mapping the whole of the fracture surface in this way it is possible to determine both the local and overall directions of crack growth. Fig. 9 demonstrates that on a local scale there are wide variations in the direction of crack growth. Some of these coincide with macroscopic features of the fracture surface, such as the steps evident at B and C in Fig. 5b, and others are associated with local variations in fibre packing and with resin-rich regions.

In specimens which had been coated with grease along the sides of the groove to prevent acid attack it was found that on a macroscopic scale the crack front remained approximately straight, normal to the long axis of the specimen. In specimens which had not been greased, some crack growth occurred from the sides and secondary crack nucleation occurred.

The effect of G on the appearance of the fracture surfaces is illustrated in Fig. 10. Two

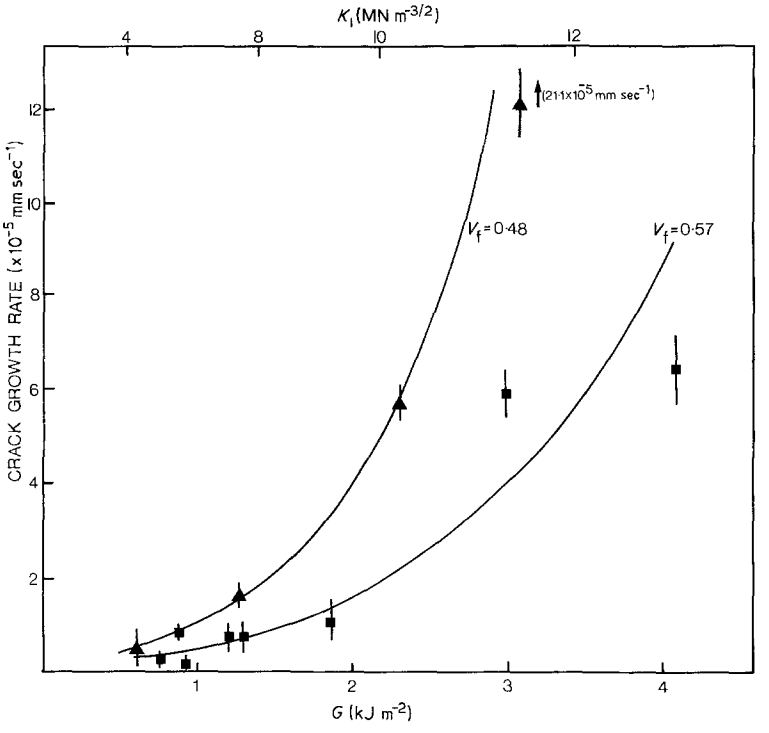

Figure 7 Effect of K_I on crack growth rate for two values of V_f.

main effects are associated with an increase in G. Firstly, the overall roughness and amount of out-of-plane fracture increases and there is a corresponding increase in the number and height of the surface steps. Secondly, the size of the mirror zones on the individual glass fibres decreases. Both these effects indicate that the stresses at the crack tip increase as G increases.

The fracture surfaces may undergo a considerable amount of post-failure damage owing to continued immersion in the acid after the crack has formed. However, it is possible to distinguish between post-failure damage and initial damage. Even short exposures of the fracture surface to acid leads to interface cracking and fibre fracture as illustrated in Fig. 11. The cracks in individual fibres on matching surfaces at A, B and C appear to be unrelated to each other and must have occurred after the main crack has formed. After long exposures to acid, extensive fibre and inter-

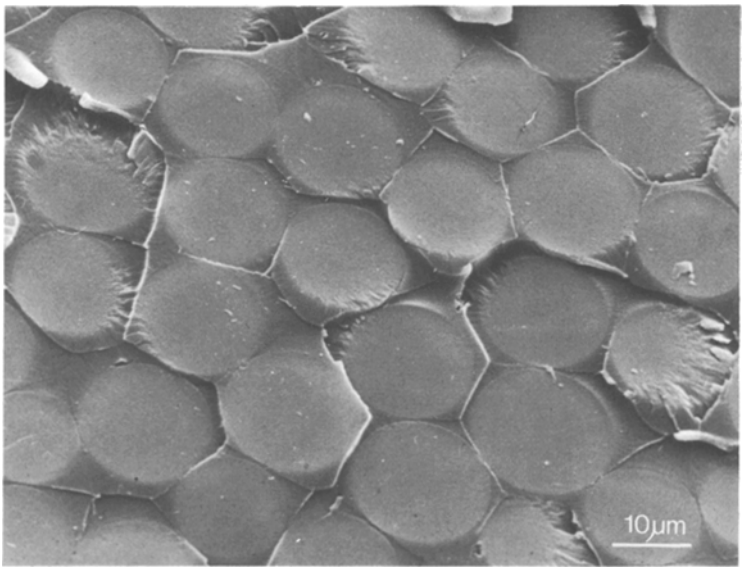

Figure 8 Scanning electron micrograph of the very smooth fracture surface in the nucleation region.

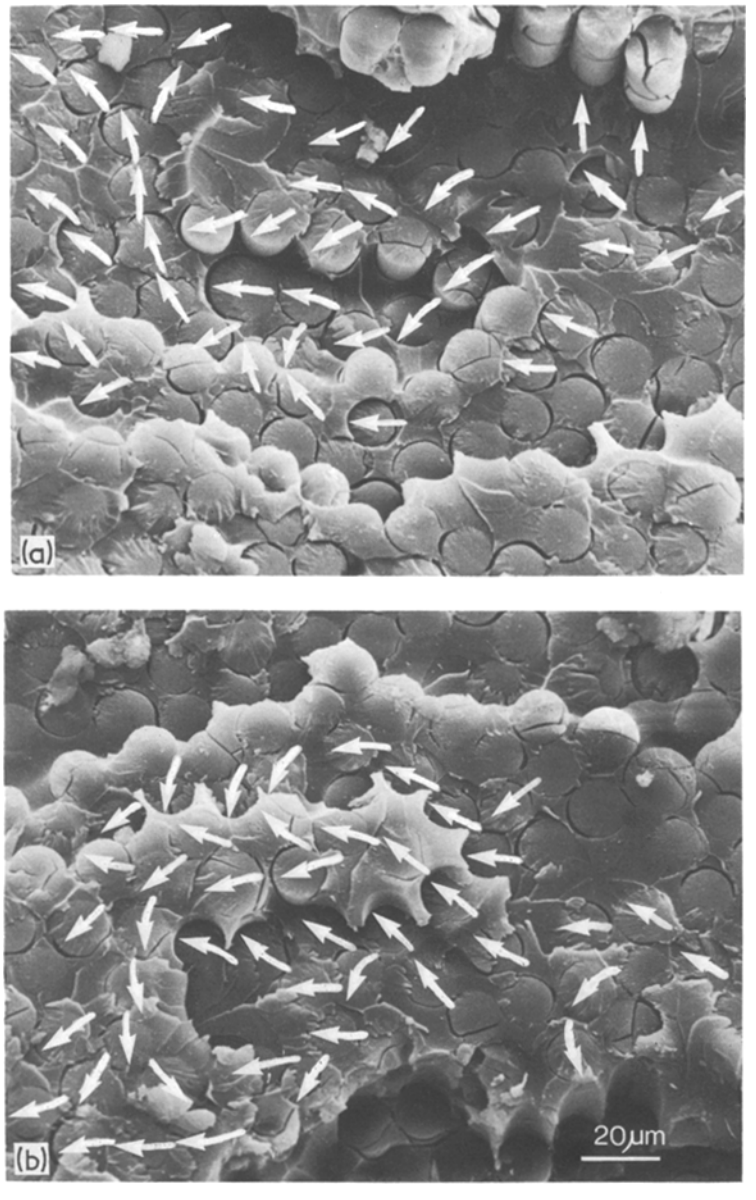

Figure 9 Scanning electron micrographs of opposite surfaces of a stress corrosion crack illustrating the local variations in crack growth direction.

face cracking develops and leaching of the fibres occurs.

5. Discussion

The detailed fractographic studies have shown that on a microstructural scale crack growth is irregular. The direction of crack growth and the shape of the crack front varies considerably from point to point. These changes are due to local variations in fibre packing and indicate that crack growth through the resin may have a significant effect on the overall crack growth rate [10]. It is not surprising, therefore, that the curves in Fig. 6 show considerable variations in da/dt even when K_I is constant. Additional variations in da/dt arise when transverse cracking occurs at the tip of the growing stress corrosion crack.

The average crack growth rates in Fig. 7 can be represented approximately by the relationship

$$V = \frac{da}{dt} = A K_I^n \qquad (6)$$

where A and n are constants. Using a linear least squares fit to plot $\log V$ against $\log K_I$ gives $n = 3.57$ and 4.22 for $V_f = 0.57$ and 0.48 respectively. The data for $V_f = 0.57$ is more complete. These results are compared with data obtained by Aveston and Sillwood [12] in Fig. 12 for tests

on similar glass–polyester resin materials in 1 N sulphuric acid. Aveston and Sillwood used parallel-sided double cantilever beam specimens so that K_I increased progressively as the crack length increased. V_f was nominally 50%. The agreement between the two sets of data in Fig. 12 is good; the curves have similar slopes ($n = 3.1$ for 1 N H_2SO_4) but are displaced relative to each other. Assuming a direct comparison can be made, it appears that da/dt in 0.6 N HCl is higher than in 1 N H_2SO_4 for a given K_I.

The changes in the appearance of the fracture surface with increasing K_I are consistent with the model for stress corrosion cracking proposed by Hogg and Hull [8]. At high values of K_I there are many of the features associated with fracture in air, such as debonding and fibre pull-out. At very high K_I the role of the environment will be negligible. However, it is unlikely that extensive crack growth will occur because of the intervention of other fracture processes. The Hogg and Hull model envisages that the presence of the acid results in fibre fracture at stresses below those in air and that when the fibre fails the crack runs through the surrounding matrix until it meets another fibre where the process is repeated. Under these conditions the overall crack growth rate is determined by the fracture toughness of the resin and the rate of acid attack on the fibres.

When K_I is reduced to very low values a point should be reached when spontaneous cracking of the resin does not occur because the local value of

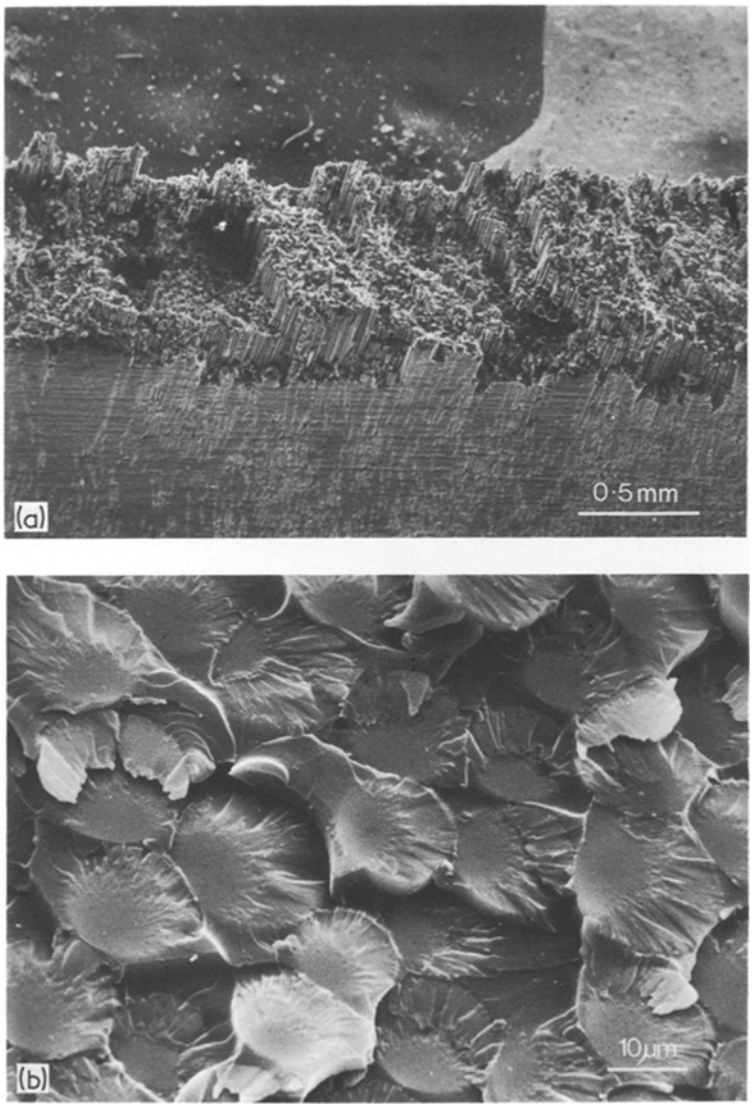

Figure 10 Scanning electron micrographs showing the effect of G on the appearance of the fracture surface. (a) and (b) $G = 1.3\,kJ\,m^{-2}$, (c) and (d) $G = 4.2\,kJ\,m^{-2}$.

Figure 10 Continued.

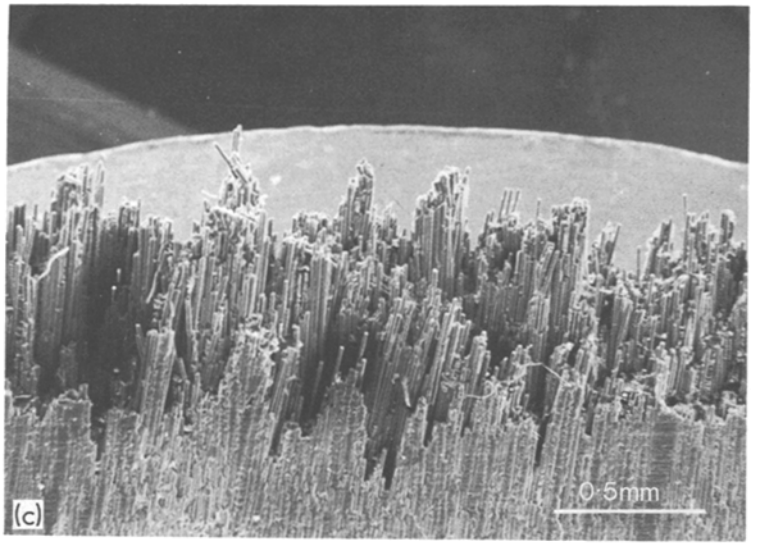

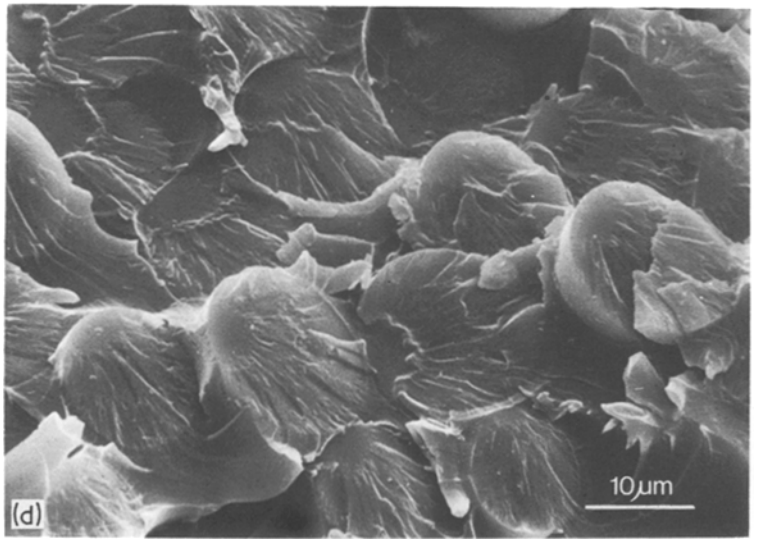

K_I is less than the resin toughness. The rate of crack growth will depend then on the diffusion rate of active ions through the resin. Failure of surrounding fibres will produce an increase in K_I acting on the intervening web of resin causing it to fail. Direct evidence for this process has been reported by Hogg and Hull [10] for stress corrosion in GRP fabricated from high toughness resins. It is anticipated that, under these circumstances, a change in n will occur. Aveston and Sillwood [12] observed some deviation of the $\log V$–$\log K_I$ curve at low values of K_I and suggested that this could be due to a stress corrosion limit as reported by Collins [15]. However, their data could be explained equally well in terms of an increase in n at low K_I.

The shape of the $\log V$–$\log K_I$ diagram is important in predicting the time to failure of GRP structures. Aveston and Sillwood [12] have successfully predicted the stress dependence of the lifetime t_c of unidirectional rods using the relation [16]

$$t_c = \frac{2K_{Ii}^{(2-n)}}{(n-2)A\sigma^2 Y^2} \tag{7}$$

where K_{Ii} is the value of K_I at an initial flaw size $a = a_i$, Y is a geometrical parameter and σ is the applied stress. However, to explain their results they assume $a_i = 0.14$ mm. Clearly, such flaws do not exist and it is postulated that a crack of this size forms easily by nucleation and growth within a fibre bundle and is stopped by a resin-rich region

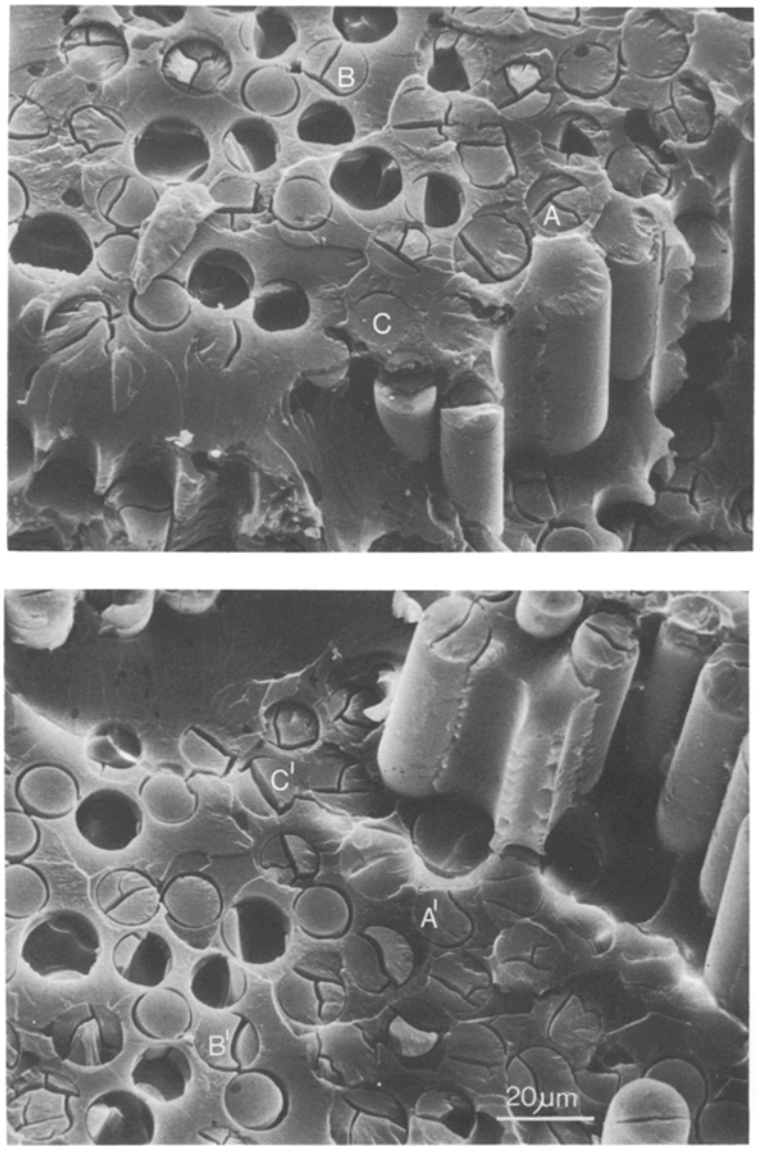

Figure 11 Scanning electron micrographs illustrating post-failure damage on matching surfaces.

around the bundle. No microscopic evidence is given and it must be noted that the predicted value of a_i is very sensitive to n in Equation 6.

The concept of an initial flaw size is of interest with regard to the lower end of the log V–log K_I curve and the possiblility of a threshold K_I for stress corrosion cracking. No evidence for resin-rich regions between bundles was found in polished sections in the present work. However, the fracture surfaces in the nucleation region (see Fig.8) were different from those in the main crack growth region. The size of the nucleation region depended on the initial load and was not related to the bundle size.

The fracture surface markings in the nucleation region suggest that the fracture mechanisms at low growth rates are different from those operating at higher values of K_I. It follows that the lifetime of a flaw-free structure will involve two stages; firstly, the time to nucleate a crack, and secondly, the time to grow the crack by conventional stress corrosion mechanisms. Both of these will depend on the initial load. The data in Fig. 6 show that at low loads there is an incubation period before macroscopic crack growth occurs.

The measurement of crack growth rates using the type of approach described in this paper is directly relevant to the prediction of failure in composite structures. It also provides a rigorous method of evaluating the effect of material vari-

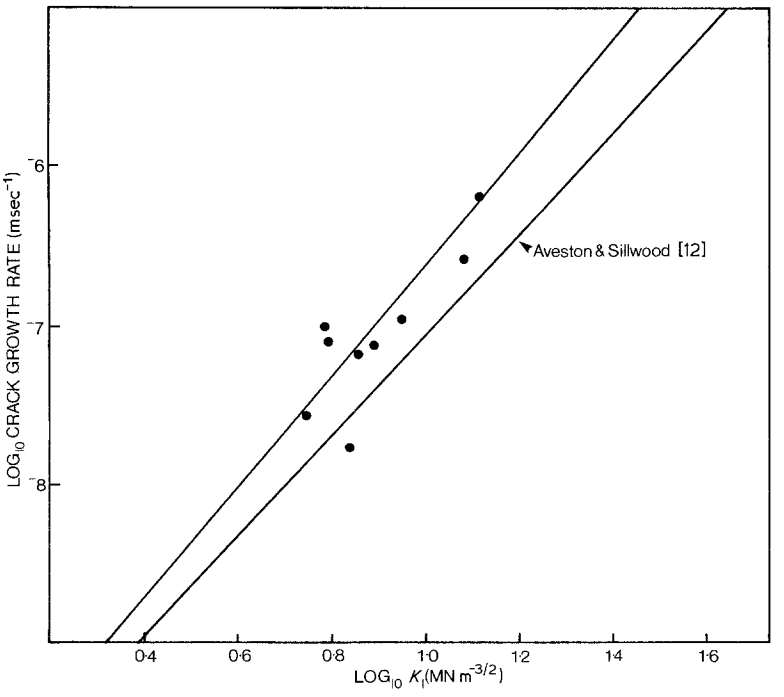

Figure 12 Comparison of V against K_I data obtained in the present work with results from [12].

ables on stress corrosion cracking. Currently experiments are in hand on the effect of resin matrix properties on unidirectional laminae and chopped strand mat.

6. Conclusions

1. Stress corrosion cracking has been observed at right angles to the fibre direction in aligned GRP at stress intensities as low as $4\,MN\,m^{-3/2}$. The corresponding crack growth rate was 1×10^{-8} m sec^{-1}.

2. The degree of out-of-plane fibre fracture and overall roughness of the fracture surface increases with increasing stress intensity. The size of the mirror zones on the individual glass fibres decreases with increasing stress intensity.

3. Nucleation of stress corrosion cracks may take considerable time when the applied stress is low. This corresponds to very slow crack growth, i.e. less than 1×10^{-8} m sec^{-1}. The fracture surfaces in the nucleation region are very smooth with large mirror zones, suggesting that a different mechanism is operating.

4. The threshold stress intensity for stress corrosion cracking will depend on the nucleation process.

Acknowledgements

We are grateful to Dr P. J. Hogg and Mr C. H. Gatward for many useful discussions, to Mr D. Taylor for assistance with the experimental work, to Mr D. Whitehurst and his colleagues for building the experimental facilities, and to the Science and Engineering Research Council for their financial support.

References

1. A. G. METCALFE, M. E. GULDEN and G. K. SCHMITZ, *Glass Technol.* **12** (1971) 15.
2. A. G. METCALFE and G. K. SCHMITZ, *ibid.* **13** (1972) 5.
3. R. J. CHARLES, *J. Appl. Phys.* **29** (1958) 1529.
4. S. M. WEIDERHORN and L. H. BOLZ, *J. Amer. Ceram. Soc.* **50** (1970) 543.
5. S. TORP and R. ARVESEN, 34th Annual Technical Conference, Reinforced Plastics/Composites Institute, Washington, February 1979 (Society of Plastics Industry, New York, 1979) Section 13-D, p. 1.
6. G. K. SCHMITZ and A. G. METCALFE, *I. EC Prod. Res. Dev.* **5** (1966) 1.
7. J. AVESTON, A. KELLY and J. M. SILLWOOD, in "Advances in Composite Materials" Vol. 1, edited by A. R. Bunsell, C. Bathias, A. Martrenchar, D. Menkes and G. Verchery, (Pergamon Press, New York, 1980) p. 556.
8. P. J. HOGG and D. HULL, *Met. Sci.* **14** (1980) 441.
9. D. HULL and P. J. HOGG, in "Advances in Composite Materials" Vol. 1, edited by A. R. Bunsell, C. Bathias, A. Martrenchar, D. Menkes and G. Verchery (Pergamon Press, New York, 1980) p. 543.
10. P. J. HOGG and D. HULL, The British Plastics Federation, 13th Reinforced Plastics Congress, Brighton, November, (The British Plastics Federation, London, 1982) p. 115.

11. M. F. KANNINEN, E. F. RYBICKI and H. F. BRINSON, *Composites* 8 (1977) 17.
12. J. AVESTON and J. M. SILLWOOD, *J. Mater. Sci.* **17** (1982) 3491.
13. D. HULL, M. J. LEGG and B. SPENCER, *Composites* **9** (1978) 17.
14. P. J. HOGG, D. HULL and B. SPENCER, *ibid.* **12** (1981) 166.
15. H. H. COLLINS, *Plast. Rubber: Mater. Applic.* **3** (1978) 6.
16. A. G. EVANS, *J. Mater. Sci.* 7 (1972) 1137.

Received 4 February
and accepted 15 February 1983